Acta Crystallographica Section D
Biological Crystallography
ISSN 0907-4449

Mosaic spread characterization of microgravity-grown tetragonal lysozyme single crystals

F. Otálora,[a]* B. Capelle,[b] A. Ducruix[c] and J. M. García-Ruiz[a]

[a]Laboratorio de Estudios Cristalográficos (IACT), CSIC-Universidad de Granada, LEC/IACT, Campus Fuentenueva s/n (Fac. Ciencias), 18002 Granada, Spain, [b]Laboratoire de Mineralogie-Cristallographie, URA 009 CNRS, Paris, France, and [c]LEBS-CNRS, Batiment 34, CNRS, 91198 Gif sur Yvette CEDEX, France

Correspondence e-mail: otalora@goliat.ugr.es

Received 15 July 1998
Accepted 5 November 1998

Mosaic spread values for crystals grown in microgravity were measured using synchrotron radiation. Full width at half maximum (FWHM) values for diffraction line profiles in the range 10–20″ (arc seconds, 1″ = 1°/3600) were observed. These values are similar to those measured for crystals grown on earth using the gel-acupuncture method. The crystals analysed are composed of from two to five domains producing peaks having widths from 5 to 15″. The distribution of these domains is neither homogeneous (with domains of lower quality concentrated in the centre of the crystal) nor isotropic (producing peaks whose width changes depending on the observation direction). Methodological aspects are also discussed, with special consideration of the effects of mosaic spread on the data-collection procedures for high-resolution (low-intensity) reflections.

1. Introduction

In recent years, mosaicity [defined as the full width at half maximum (FWHM) of Bragg diffraction profiles] has been used as a criterion for the assessment of the quality of protein crystals (Helliwell, 1988; Fourme *et al.*, 1995; Helliwell *et al.*, 1995; Snell, Weisgerber *et al.*, 1995; Ferrer *et al.*, 1996). Simply stated, mosaicity reflects the departure from perfection of the crystal lattice. This imperfection arises from several features of the crystals, notably their mosaic structure (the fact that the crystal volume is not a continuous lattice but is composed of small blocks that are slightly misaligned) and the presence of defects which disturb the lattice geometry. Several methods are used to measure this parameter, all based on measuring the FWHM of diffraction spots. These methods can be classified in peak-profile analysis (when the peak is scanned by moving the crystal, the point detector or both, producing a one-dimensional profile or a two- or three-dimensional mapping) and spot-profile analysis (when the intensity distribution is spatially resolved using a two-dimensional detector). Usually, in spot-profile methods in protein crystallography the projection of the diffraction spot is obtained using monochromatic (usually screenless rotation) or polychromatic (Laue) methods. Because the defect structure provokes a spread of the diffracted intensity around the reciprocal-lattice nodes, the recorded spots are a more or less deformed image of the crystal, with an intensity distribution controlled by the size and misalignment of the different domains making up the whole crystal volume. On the other hand, peak-profile methods are based on recording, using a point detector, the intensity diffracted by a single spot as the corresponding reciprocal-lattice node goes through the Ewald sphere. In both cases, the spot or peak acquired is the convolution of several

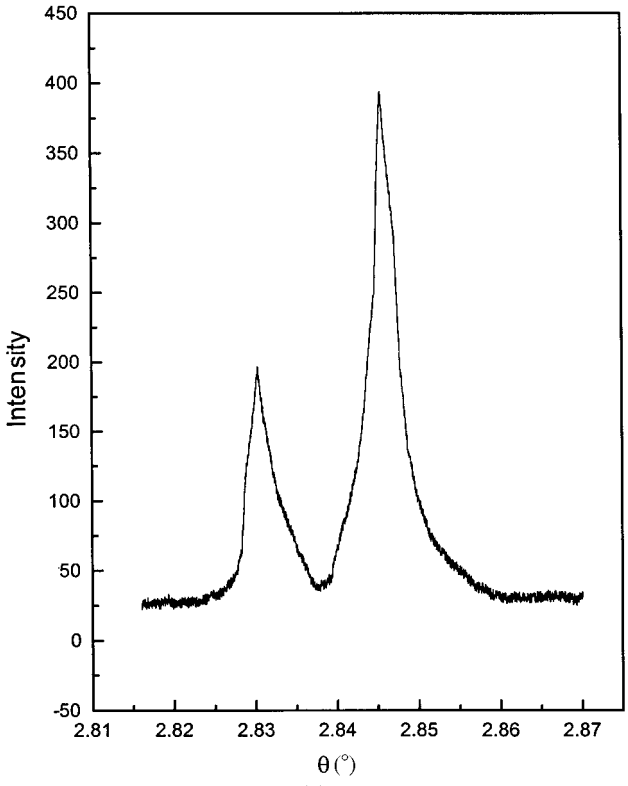

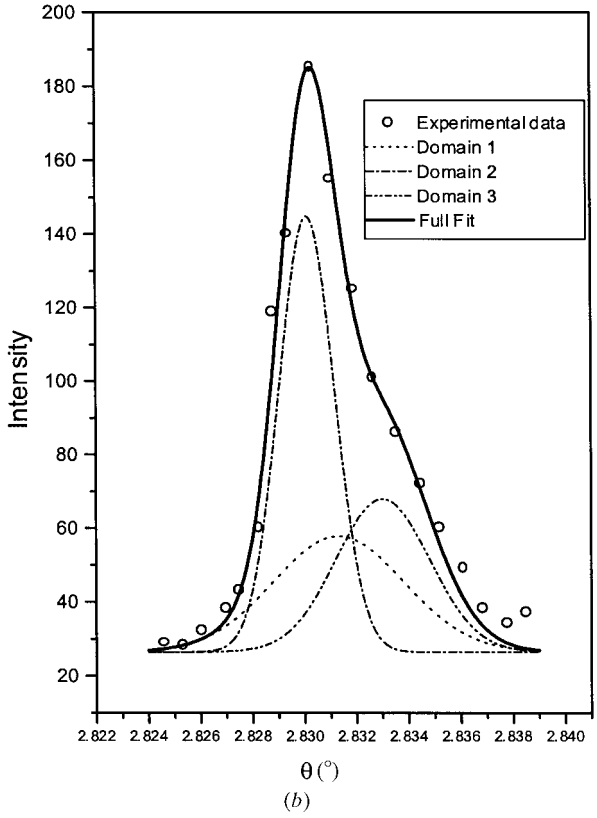

Figure 1
(*a*) Diffraction spot recorded from a lysozyme crystal grown on earth (gel-acupuncture method). This crystal presented a small crack that produces the splitting of the peak. (*b*) Plot showing the fitting of the smaller peak to the sum of three Gaussian domain peaks.

distributions: the intrinsic profile width, the experimental width and the mosaic spread. The dynamical theory of diffraction (Laue, 1960) states that a perfect crystal produces diffractions having an intrinsic width that is basically a function of experimental factors (such as the wavelength and orientation of the crystal with reference to the incident and diffracted beams) and the properties of the crystal (structure factors and unit-cell volume; for details see Helliwell, 1988; Fourme *et al.*, 1995). These theoretical rocking widths for perfect protein crystals are typically close to 1″ (Helliwell, 1988). This distribution is blurred by some experimental factors, mainly beam divergence, bandwidth and source size. As vertical divergence for synchrotron sources is much lower than horizontal divergence, peak-profile methods are almost insensitive to beam-divergence effects when the scan is performed around a horizontal rotation axis perpendicular to the incident beam. The bandwidth ('monochromaticity') effect must be reduced using high-performance monochromators with very small intrinsic widths. A further effect that blurs the intensity distributions is the point spread function (PSF) of two-dimensional detectors (Bourgeois *et al.*, 1994), which only affects spot-profile methods, especially when detectors with large PSF (such as image plates) are used. Summing up, the FWHM of the recorded profile includes contributions from (i) the mosaic spread (rocking width) of the crystal (*i.e.* the quantity we are interested in), (ii) the intrinsic rocking width of the crystal and (iii) experimental distributions mainly controlled by the divergence and bandwidth of the source, the characteristics of the monochromator, the geometry of the experimental set-up and the PSF of the detector (depending on which detector is used). All these contributions were taken into account when selecting the experimental setup used in this work (see §2).

The anatomy of a diffraction peak profile (Fig. 1) acquired from a protein single crystal contains information on different scales. At the scale of $10^{-1\circ}$ (360″), the profile consists of the superimposition of several 'crystal peaks' contributed by different parts of the crystal separated by cracks or by severely bent volumes. Fig. 1(*a*) shows a split peak corresponding to a diffraction spot from a lysozyme crystal containing a crack. The two crystal peaks correspond to diffraction from the two parts separated by the crack and each has an integrated intensity proportional to the volume of the corresponding part of the crystal. Note the horizontal scale: the whole figure covers $5 \times 10^{-2\circ}$, which corresponds to three pixels (each 0.15 mm) of a 2000 pixel resolution 30 cm diameter area detector at a distance of 50 cm from the crystal. The width of each such crystal peak is of the order of $10^{-2\circ}$. These crystal peaks can be the sum of several 'domain peaks' on the $10^{-3\circ}$ scale. Such domains are the most perfect piece of crystal we can distinguish from peak profiles, but still contain 'defects' which make the width of the domain peaks significantly larger than the theoretical width of a perfect three-dimensional protein crystal lattice, estimated to be close to 1″ (Helliwell, 1988). Fig. 1(*b*) shows the domain peaks which make up the crystal peak on the left in Fig. 1(*a*). Data points at the right side of the plot do not follow the fit because of the influence of

the neighbouring peak (the fit has been calculated for both peaks but is shown only for the one on the left). Good protein crystals do not normally show cracks or severe bending and we will therefore concentrate on the crystal and domain peaks, *i.e.* on 'sub $10^{-2\circ}$' scales, although continuously bent crystals can produce the same features on larger scales.

2. Experimental

Crystals analysed in this work were obtained from two growth experiments performed inside APCF 200 µl FID reactors (Bosch *et al.*, 1992) during the LMS mission of the ESA on the NASA Space Shuttle (STS-78 mission). Both experiments were performed using 10%(*w*/*v*) NaCl solution as the precipitating agent and 100 mg ml^{-1} lysozyme solution. The reactors were used in FID mode without any membrane. The only difference between the two experiments was the use of five flat capillaries inside the protein chamber of one of the reactors, which was intended to force crystal growth inside the capillaries in order to reduce mechanical stress during landing and to avoid crystal handling during mounting. The resolution limit for these crystals has been measured at station W32 at LURE, the average resolution limit for the crystals analysed being about 1.25 Å.

Peak profiles for diffraction spots at 3 Å resolution were measured at station D25b (beamline D2 of the DCI positron storage ring at LURE). This station features a double-crystal spectrometer in which the first crystal is the monochromator and the second one is the sample itself. The advantages of this station for mosaicity measurement have been discussed previously (Fourme *et al.*, 1995), so we will only highlight the extremely low vertical divergence and bandwidth, the very high resolution goniometer and the possibility of on-line observation of the crystal during measurement by using an X-ray absorption camera in the path of the direct beam after the crystal. During the experiments reported here, we used a four-reflection (three symmetric) Si(111) monochromator (d = 3.1353 Å) oriented to reflect in the vertical plane. The wavelength was adjusted to 1.2 Å (11.033°). The NaI scintillation detector was set at $2\theta = 22.07^\circ$ to work in a symmetrical setting (recording diffractions having the same spacing as the monochromator minimizes experimental contributions to the profile width). Using this combination of monochromator and recording geometry, a total experimental width of only 0.8″ is convolved with the recorded peaks. All widths in this work are reported without correction for this experimental width. For profile acquisition, an automated procedure was followed performing several scans using a piezoelectric device under computer control; the resulting profiles were summed to enhance counting statistics after correcting for mechanical and thermal drift of the instrument. Peak profiles acquired were fitted as the addition of several (from two to four) Gaussian functions

$$y = y_0 + \frac{A}{w(\pi/2)^{1/2}} \exp\{-2[(x - x_c)/w]^2\},$$

where y_0 is an offset (background noise level), A is the area (integrated intensity) of the peak, w is the width (mosaic spread) and x_c is the angular coordinate of the maximum (Bragg angle). Lorentzian functions were also tested, but they produced fits of lower quality. The use of more complex functions was disregarded owing to the very good fit of data to the simple Gaussian functions. During the fit, we started with the minimum possible number of Gaussians that were evident from the shape of the peak (usually 2). These Gaussians are interpreted as domain peaks. The residuals of the fit were then checked, looking for additional minor Gaussians contributing to the peak shape. We were always cautious when the automatic fit procedure produced too many or too narrow Gaussians.

3. Results

Very small mosaicity values were found. All peaks showed non-corrected FWHM ranging from 10 to 20″. All these peaks were fitted to the addition of two to four domain peaks. The width of these components ranges from 4.5 to 15″.

Fig. 2(*a*) shows a crystal peak with FWHM = 10.5″. This crystal peak is composed of only two domain peaks, having widths of 6.1 and 12.3″. The integrated intensities of these domain peaks are 17165 counts s^{-1} for the narrow peak and 26311 counts s^{-1} for the wide peak (a ratio of 0.65). The

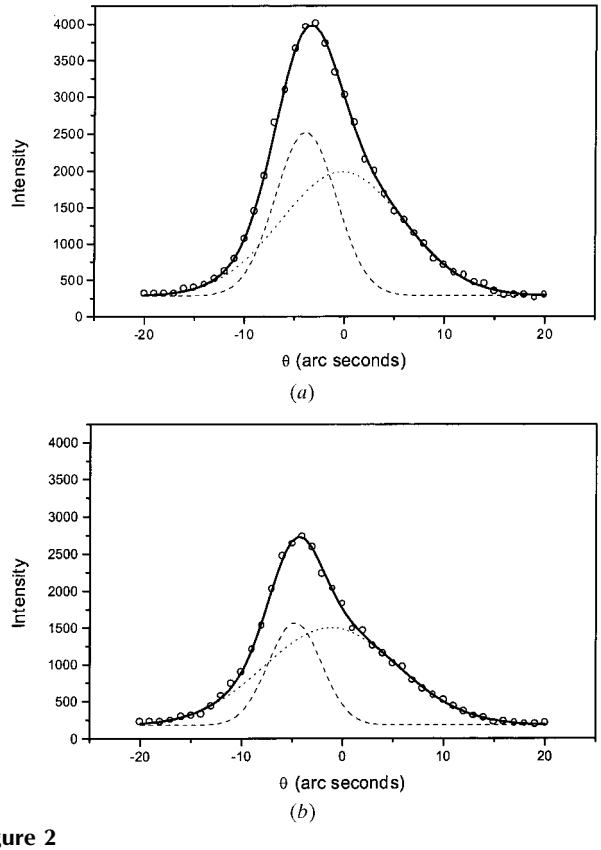

Figure 2
Peak profile of a diffraction peak from a space-grown lysozyme crystal (FID). (*a*) Profile recorded when the whole crystal is exposed. (*b*) Profile recorded exposing only the central part of the crystal.

volume of the crystal is composed of two mosaic blocks, although no conclusions can be derived in terms of their nature and defect structure except that they are not perfect mosaic domains. Fig. 2(*b*) shows the profile of the same peak after narrowing the beam to illuminate only the central part of the crystal. This narrowing is achieved by displacing the two pairs of slits while controlling the beam size and position using an X-ray absorption camera. This peak records only the contribution of the central part of the crystal. The position and width of the two domain peaks are very similar (5.2 and 13.2″), but their relative intensity has changed to 9131 counts s^{-1} for the narrow peak and 21858 counts s^{-1} for the wide peak (a ratio of 0.42). This means that the two domains are not homogeneously distributed over the crystal volume, the parts of lower quality being concentrated close to the centre of the crystal. This is reasonable since the growth rate of these crystals changes with time (Otálora, Novella *et al.*, 1999), being faster at the beginning of the experiment (while the centre of the crystal is growing). It has previously been shown that the domains of different quality making up a lysozyme single crystal are not homogeneously distributed (Otálora *et al.*, 1996; Higuchi *et al.*, 1996) and that this inhomogeneity can be caused by differences in growth rates. Fig. 3 shows $I_{\rm total}/I_{\rm centre}$ *versus* the width of the domain peak plot for different domain peaks ($I_{\rm total}$ being the diffracted intensity recorded when exposing the whole crystal and $I_{\rm centre}$ being the intensity when only the centre of the crystal is exposed). The X-ray absorption image was used to ensure the relative positioning of the crystal and the incident beam. This figure clearly shows that the intensity reduction is larger for narrow peaks than for wider ones and, therefore, that the average quality of the central zones of the crystals is lower than that of peripheral zones.

Different crystals obtained from the same experiment show different numbers of domain peaks, although the average width of these components is in the same range. Fig. 4(*a*) shows the peak profile of a crystal from the same experiment as that illustrated in Fig. 2. This profile has a FWHM of 13.8″ and is composed of four Gaussians of widths 14.5, 8.13, 6.4 and 4.6″. After acquiring this profile, we rotated the crystal by 80° (the limit of the goniometer) and recorded another spot at the same resolution (3 Å). This peak is illustrated in Fig. 4(*b*). Large differences are observed between the two crystal peaks. It is immediately clear that the peak illustrated in Fig. 4(*b*) is much wider (27.0″). This means that the mosaicity and possibly also the internal defect structure of each block are anisotropic properties. The same domain peak can show different widths when measured from different crystallographic directions. This obviously also implies differences in height, though the amplitude, which is proportional to the domain volume, is the same. The relative positions of these

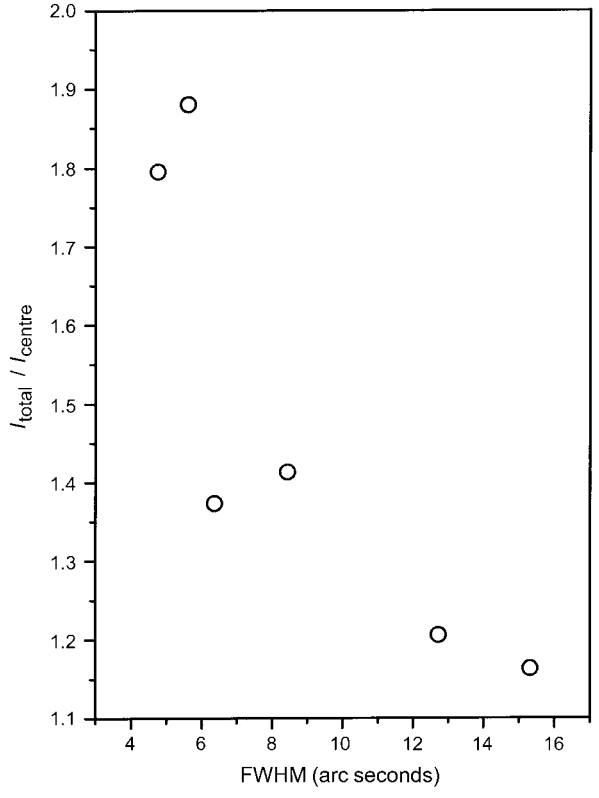

Figure 3
$I_{\rm total}/I_{\rm centre}$ ratio *versus* the width of the domain plot for various crystals grown in microgravity. $I_{\rm total}$ is the integrated intensity recorded exposing the whole crystal and $I_{\rm centre}$ the integrated intensity collected from the central part of the crystal.

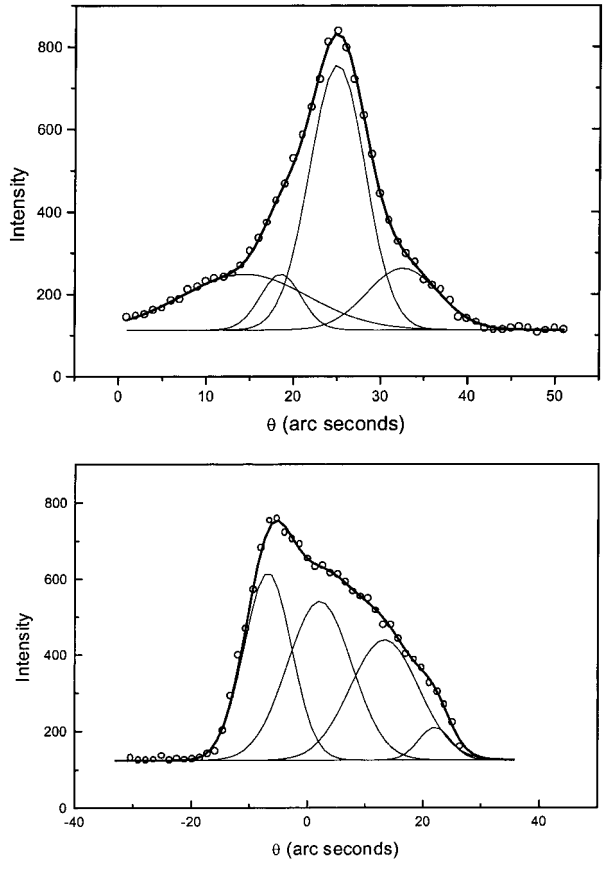

Figure 4
Profile of two spots obtained from the same crystal. The spots were recorded at θ angles differing by 80°.

domain peaks changes depending on the crystallographic directions, producing crystal peaks of different width. Anisotropy in the width of domain peaks can arise from the accumulation of one- or two-dimensional crystal defects in a given direction or by differences in the mechanical properties of the crystal lattice, which could produce a microbending of different amplitude depending on the crystallographic orientation.

4. Discussion and conclusions

Peak-profile analysis at synchrotron stations (very low bandwidth, vertical divergence almost zero) equipped with high-resolution goniometers (at the level of 0.1″ per step or less) and very low rocking width monochromators is the best way to obtain data accurate enough to understand (not simply measure) the mosaicity and the defect structure of protein single crystals. Methods based on image analysis of two-dimensional detectors are generally not accurate enough, owing to the spatial resolution and to the point-spread function (PSF) of the detector (specially CCD and image plates) which produces a blurring of the spot. Long-distance Laue diffraction (Snell, Habash *et al.*, 1995) and the use of film as a two-dimensional detector have been proposed as adequate spot-profile techniques for crystal quality assessment.

The angle sustained by a single pixel on an area detector having 30 cm diameter and 2000 pixel resolution (150 μm pixel size) located 1 m from the crystal is about 30″, larger than all the rocking widths measured during this study. The PSF of CCD and IP detectors currently used is about 1 mm at 0.1% of peak maximum (Bourgeois *et al.*, 1994). This means that the 'true' peak profile (convolution of the sample mosaicity, intrinsic width and experimental factors) having a sub-pixel size is convolved with a PSF of about 2 pixels FWHM. Therefore, mosaicity should have no influence on the quality of diffraction data sets collected using current procedures (oscillation technique and current CCD or image-plate detectors), because the intensity spread over neighbouring pixels arising from the mosaic spread is much lower than that produced by the PSF of the detector. For successive images recorded by scanning the reciprocal space, reducing the oscillation range for individual images (fine slicing) is known to increase the signal-to-noise ratio of spots. In this case, the reduction of mosaic spread would reduce the number of partials and increase the signal-to-noise ratio. Fig. 5 shows (open circles) the better (theoretical) signal-to-noise value (as a function of the oscillation range) numerically computed assuming the oscillation of a crystal from which a Gaussian peak $10^{-3\circ}$ wide, ten times higher than the background and centred in the oscillation range is collected. This ratio continuously increases as the oscillation range decreases. Unfortunately, the number of slices needed to collect a full data set also increases, as well as the storage and number-crunching needs. The solid line in Fig. 5 shows the storage capacity (in gigabytes) needed to store a 90° image set as a function of the oscillation range. Processing time increases (at best) in the same way. Therefore, it is clear that obtaining better data by using fine-slicing oscillation and very low mosaicity crystals is theoretically feasible, but beyond the limits of currently available computer technologies. However, both detector and computer technologies are very rapidly evolving, and this discussion may become outdated very soon.

Independently of the technique used, experimental parameters like beam divergence and bandwidth must be taken into account. Details on how to optimize these parameters at station D25 are discussed in Fourme *et al.* (1995). The experimental width convolved with the sample width using the geometry selected can be estimated to be 0.8″. Taking into account that the intrinsic width of a perfect lysozyme crystal can be estimated to be of the order of 1″ (Helliwell, 1988) and that the best domain peaks found here have a width of about 5″, it is clear that these profiles indicate the presence of some kind of further defect structure such as a given concentration of discrete crystalline defects or a continuous bending of the crystal structure on the scale of a few arc seconds. This second possibility seems to be coherent with the mechanical properties of protein crystals and with the absence of sharp domain boundaries in most topographs recorded from good lysozyme crystals. This kind of topographic images could be of great interest, in conjunction with peak profiles, in determining the number and position of mosaic domains and in understanding the intradomain defect structure. To improve the usefulness of this kind of image, shaped protein crystals such as those obtained by the gel-acupuncture technique (Otálora *et al.*, 1996) could be used. Large crystals grown inside flat capillaries are the most suitable samples for this kind of analysis, but none of the crystals obtained from the APCF reactor containing such capillaries was large enough to completely fill the capillary and acquire the plate shape needed. An example of this kind of topographic studies is presented in Otálora, García-Ruiz *et al.* (1999).

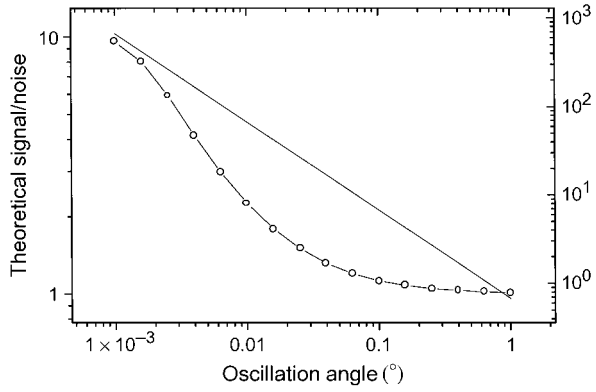

Figure 5
Theoretical value for the signal-to-noise ratio as a function of the oscillation range in fine-slicing data collection (empty circles). The intensity produced by scanning a 3.6″ ($10^{-3\circ}$) wide peak centred in the oscillation range and having a noise background ten times lower than the peak maximum is integrated for different oscillation angles and divided by the intensity produced by the same scan over the background. The amount of storage needed to collect a 90° oscillation image set using a 2000 × 2000 pixel resolution detector using current technology is also plotted (solid line).

These lysozyme crystals seem to be composed of several slightly defective mosaic domains, ranging from two to four for the samples examined. Very small mosaicity values have been found. All peaks show FWHM ranging from 10 to 20″ and are composed of at least two domains having FWHM as low as 5″ (without correction). These values are comparable with those found for crystals grown on earth by the gel-acupuncture method. Fig. 6 shows a diffraction peak obtained from a lysozyme crystal grown by this method using 200 mg ml^{-1} lysozyme and 20%(*w*/*v*) NaCl solutions. The FWHM of this peak is 11″ and it is composed of three domain peaks, the width of the most intense being 9″. Therefore, in this case no advantages seem to be derived from the microgravity growth of lysozyme in terms of mosaicity. Since mosaicity is mainly controlled by the density and nature of crystalline defects in the crystal and this concentration is mainly a function of the growth rate, this result is consistent with the large initial growth rates measured in lysozyme crystal-growth experiments in the APCF (Otálora, Novella *et al.*, 1999) and with the mixed regime for lysozyme growth kinetics (Vekilov *et al.*, 1996), which provokes large fluctuations in growth rates. This result cannot necessarily be interpreted to disfavour microgravity experiments, as no relation has yet been stated between mosaicity and resolution limit. More experimentation in microgravity crystal growth is needed to supplement our present knowledge on this problem, including the systematic determination of accurate resolution limits and mosaicity values for different macromolecules growing under different kinetic regimes.

Mosaicity can be an inhomogeneous and anisotropic property. Domains of different quality are not homogeneously distributed. The central part of the crystals analysed, which grows at a faster rate, accumulates the domains having higher mosaicity. This observation supports the previously reported dependence of mosaicity values on the local growth rate (Otálora *et al.*, 1996). We found large FWHM differences for peaks collected at the same 2θ angles (*i.e.* resolution) in the same crystal observed from different orientations. This proves that mosaicity can be anisotropic. This anisotropy can arise from orientation-dependent differences in the width of domain peaks contributing to the shape of the whole peak or from an anisotropy in the angular misorientation between different domains. If all unit cells in a crystal are perfectly aligned, the structure-factor distribution can be visualized as centred at the nodes of the reciprocal-space lattice and having a width ω that is the convolution of the intrinsic width and the experimental width. If the crystal is composed of several blocks that are slightly misaligned, these misalignment angles modify the structure-factor distribution around the reciprocal-lattice nodes and the spot will be composed of several superimposed intensity distributions having their centres displaced and an integrated intensity proportional to the volume of each mosaic domain. To analyse a simple case, suppose a crystal composed of two crystal domains misaligned by a rotation of η° around the [010] direction. In this situation, spots 100 and 001 will display two separate domain peaks if we record a θ scan around the [010] direction and both domain peaks will be superimposed and not detected if the θ scan is around the [100] or [001] directions. Therefore, depending on the spot selected and the scanning axis, it is possible to measure any mosaicity value between ω and $\omega + \eta$.

The experiments in microgravity (as well as those on earth) described here were performed using lysozyme from Sigma without further purification. Further enhancement in the mosaicity values is expected on using protein of very high purity.

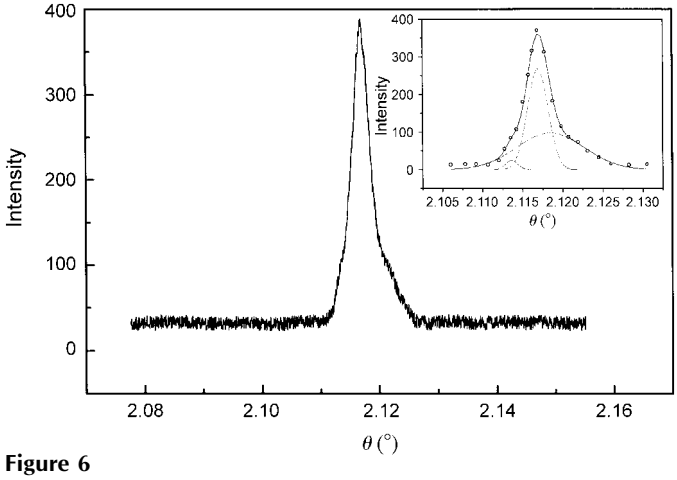

Figure 6
Profile of a diffraction spot recorded from a lysozyme single-crystal grown on earth (gel-acupuncture method). The FWHM of the whole peak is 11″ (0.003°).

References

Bosch, R., Lautenschlager, P., Potthast, L. & Stapelman, J. (1992). *J. Cryst. Growth*, **122**, 310–316.

Bourgeois, D., Moy, J. P., Svensson, S. O. & Kvick, Å. (1994). *J. Appl. Cryst.* **27**, 868–877.

Ferrer, J. L., Hirschler, J., Roth, M. & Fontecilla-Camps, J. C. (1996). *ESRF Newslett.* June 1996, 27–29.

Fourme, R., Ducruix, A., Riès-Kautt, M. & Capelle, B. (1995). *J. Synchrotron Rad.* **2**, 136–142.

Helliwell, J. R. (1988). *J. Cryst. Growth*, **90**, 259–272.

Helliwell, J. R., Snell, E. & Weisgerber, S. (1995). *Proceedings of the IXth European Symposium on Gravity Dependent Phenomena in Physical Sciences*, edited by L. Ratke, H. Walter & B. Feuerbacher, pp. 155–170. Berlin: Springer Verlag.

Higuchi, Y., Okamoto, T. & Yasuoka, N. (1996). *J. Cryst. Growth*, **168**, 99–105.

Laue, M. von (1960). *Röntgenstrahl-Interferencen.* Frankfurt-Am-Main: Akedemische Verlag.

Otálora, F., García-Ruiz, J. M., Gavira, J. A. & Capelle, B. (1999). *J. Cryst. Growth*, **196**(2–4), 546–558.

Otálora, F., Moreno, A. & García-Ruiz, J. M. (1996). *J. Cryst. Growth*, **168**, 93–98.

Otálora, F., Novella, M. L., Rondón, D. & García-Ruiz, J. M. (1999). *J. Cryst. Growth*, **196**(2–4), 649–664.

Snell, E., Habash, J., Helliwell, M., Helliwell, J. R., Raftery, J., Kaucic, V. & Campbell, J. W. (1995). *J. Synchrotron Rad.* **2**, 22–26.

Snell, E. H., Weisgerber, S. & Helliwell, J. R. (1995). *Acta Cryst.* D**51**, 1099–1102.

Vekilov, P. G., Alexander, J. I. D. & Rosenberger, F. (1996). *Phys. Rev. E*, **54**, 6650–6660.